Single Chromatin Fiber Stretching Reveals Physically Distinct Populations of Disassembly Events

L. H. Pope,* M. L. Bennink,* K. A. van Leijenhorst-Groener,* D. Nikova,* J. Greve,* and J. F. Marko†
*Biophysical Techniques, Department of Science and Technology and MESA+ Institute for Nanotechnology, University of Twente, 7500 AE Enschede, The Netherlands; and †University of Illinois at Chicago, Department of Physics, Chicago, Illinois 60607-7059 USA

ABSTRACT Eukaryotic DNA is packaged into the cell nucleus as a nucleoprotein complex, chromatin. Despite this condensed state, access to the DNA sequence must occur during gene expression and other essential genetic events. Here we employ optical tweezers stretching of reconstituted chromatin fibers to investigate the release of DNA from its protein-bound structure. Analysis of fiber length increase per unbinding event revealed discrete values of ~30 and ~60 nm. Furthermore, a loading rate analysis of the disruption forces revealed three individual energy barriers. The heights of these barriers were found to be ~20 k_BT, ~25 k_BT, and ~28 k_BT. For subsequent stretches of the fiber it was found that events corresponding to the ~28 k_BT energy barrier were significantly reduced. No correlation between energy barrier crossed and DNA length release was found. These studies clearly demonstrate that optical tweezers stretching of chromatin provides insight into the energetic penalties imposed by chromatin structure. Furthermore these studies reveal possible pathways via which chromatin may be disrupted during genetic code access.

INTRODUCTION

DNA typically undergoes a 10^4–10^5 compaction in length when packaged into the eukaryotic cell nucleus. This is achieved through DNA-protein interactions in the formation of chromatin. One major question that remains unanswered is how DNA is organized and accessed within this structure. With this question in mind, chromatin has been extensively studied using both biochemical and biophysical techniques. Through these studies the fundamental packaging unit of chromatin, the nucleosome, has been identified and subsequently extensively characterized (van Holde, 1989; Wolffe, 1995). This unit consists of a nucleosome core particle (NCP), linker histone, and linker DNA. The NCP is defined as 146 basepairs (bp) of DNA wrapped 1.65 times around a protein core consisting of eight histones (two copies of H2A, H2B, H3, and H4). Linker histones bind to the DNA entering and exiting the NCP, stabilizing a wrap of ~160 bp of DNA around the core. Nucleosomes are formed along the entire length of the genome, spaced by ~200 bp, resulting in a chromatin fiber that has a width of 11 nm.

Nucleosomal arrays are further folded and compacted to form higher order chromatin structures. The next level of compaction results in the formation of the ''30-nm'' chromatin fiber. Two models that have been proposed for this higher-order structure include a regular spiral (Finch and Klug, 1976; Widom and Klug, 1985) and an irregular zigzag (Horowitz et al., 1994; Bednar et al., 1995, 1998; Leuba et al., 1994, 1998a; Bustamante et al., 1997). Folding nucleosomal arrays to form the 30-nm fiber may be established by a number of different mechanisms. For example, histone tails that extrude from the NCP are target sites for posttranslational modifications such as acetylation and phosphorylation (van Holde, 1989). These modifications affect NCP-NCP interactions and hence may control compaction in a regulatory manner. For a recent review on nucleosome dynamics see Luger (2003). Similarly, linker histone is also thought to be important in higher-order structure (Clark and Kimura, 1990). Of further relevance is the observation that chromatin depleted in linker histone can compact simply through altering ionic conditions (Clark and Kimura, 1990; Hansen et al., 1989; Hansen and Wolffe, 1992; Garcia-Ramirez et al., 1992; Schwarz and Hansen, 1994). It hence appears that the degree of shielding of the highly charged DNA phosphodiester backbone is central to compaction and that this could be achieved not only via linker histones or core histone tails but also through binding of other small basic proteins. Indeed, chromatin is known to be rich not only in histones but also HMG proteins, which may play a role in this charge shielding (Wolffe, 1995). The role of polyamines in chromatin structure has also gathered recent interest (Laitinen et al., 1998).

The 30-nm chromatin fiber is considered as the ''active'' structural form and must hence be dynamic in nature to allow access to the genetic code for processes such as transcription, recombination, and repair whereas DNA remains largely in a packaged form. Present-day research is focusing on elucidating the mechanisms by which this is achieved. Recently, with the advent of single-molecule research, an arsenal of new techniques has become available to contribute to the study of chromatin. Unique insights into structure, mechanics, dynamics, and the kinetics of DNA-protein interactions, central to chromatin compaction, may be studied using techniques such as atomic force microscopy and optical tweezers (Cui and Bustamante, 2000; Bennink et al., 2001a;

Submitted September 16, 2004, and accepted for publication January 31, 2005.

Address reprint requests to J. F. Marko, University of Illinois at Chicago, Dept. of Physics, 845 W. Taylor St., Chicago, IL 60607-7059. Tel.: 312-996-3416; Fax: 312-996-9016; E-mail jmarko@uic.edu.

0006-3495/05/05/3572/12 $2.00

doi: 10.1529/biophysj.104.053074

Brower-Toland et al., 2002; Leuba et al., 1994, 1998a,b; Yodh et al., 2002; Nikova et al., 2004), or using flow-generated forces (Bennink et al., 2001b; Ladoux et al., 2000).

Focusing on optical tweezers studies of chromatin, three studies have been published to date. Although similar experimental techniques have been used, these studies differ widely in terms of the chromatin samples and methodology. The first study examined individual chromatin fibers extracted directly from chicken erythrocytes (Cui and Bustamante, 2000). This study focused on the mechanical properties of native chromatin in different salt conditions. The rationale for this study stemmed from the observation that chromatin is less compact in low-salt conditions, hence a comparison between extended and compact chromatin could be made. The main results from this study were a stretch modulus of 5 pN and a persistence length of 30 nm for the low-salt chromatin configuration.

The second study focused on structural information that could be gained through stretching chromatin fibers reconstituted using a *Xenopus* egg extract (Bennink et al., 2001a). This study started with single DNA molecules under nanomanipulation control as a template onto which nucleosomes were assembled. By this method, precise studies were made of a single chromatin fiber containing an a priori known and reproducible amount of DNA. This study, in contrast to the first, reported a chromatin stretch modulus of ~150 pN, notably the salt (NaCl) concentration here was 150 mM as compared to 5 mM and the chromatin fiber was different in composition. Moreover, the disruption of single nucleosomes was observed for the first time. It should be noted that this study was undertaken using one single loading rate condition.

The third study involved individual DNA molecules onto which well-defined short nucleosomal arrays were assembled, absent of linker histone (Brower-Toland et al., 2002). In contrast to the other two studies both force-clamp and velocity-clamp studies were undertaken. From the results of this study, most notably the observation of ~26 nm, ''half-nucleosome'', opening events, it was proposed that the nucleosomes were disrupted in a multistage process. Furthermore, a dynamic force microscopy study allowed an estimation of the energetic barrier of ~37 k_BT associated with one of these stages. These three studies have been discussed in detail in a recent review (Pope et al., 2002).

Here we describe our most recent optical tweezers results obtained from stretching chromatin fibers that have been reconstituted using a core-histone-rich extract from *Xenopus laevis* eggs. This reconstitution procedure is widely used since the chromatin fibers formed consist of nucleosomal arrays with the same nucleosomal spacing as in native chromatin (Glikin et al., 1984). The relevance of the artificial chromatin fiber is supported by studies that have shown that the injection of prokaryotic DNA into *Xenopus laevis* eggs results in the rapid assembly of chromatin, surrounded by both a nuclear envelope and lamina (Forbes et al., 1983). Additionally replication sites are assembled along λ-DNA by the extract clearly demonstrating that the extract assembles physiologically relevant structures independent of DNA sequence (Cox and Laskey, 1991). Biochemical characterization of the extract showed that it was rich in core histones, lacked linker histone H1 found in mature cells, but, however, did contain embryonic linker histone B4 (Smith et al., 1988). It is interesting to note that B4 is thought to provide weaker internucleosomal interactions than H1, and hence results in the formation of a chromatin fiber that is more open and extended in structure (Smith et al., 1988; Wolffe, 1995).

In this study we focused primarily on the response of reconstituted chromatin fibers to a range of different loading rate conditions to gain insight into the energetic penalties imposed by chromatin structure. Dynamic force spectroscopy theory (Evans, 1999, 2001; Evans and Ritchie, 1997, 1999) considers that the disruption of two interacting biomolecules may require the crossing of one or more energy barriers and that these barriers will be reduced in size through force-induced disruption. In an unperturbed system energy barriers are crossed simply through thermal fluctuations, hence interactions have characteristic dissociation kinetics, which are governed by the size, shape, and location of these barriers. Applying force to the intermolecular bonds tilts the energy landscape that describes these interactions, and the rate at which tilting occurs is dependent on the rate at which force is applied (loading rate). For a single energy barrier theory predicts a scaling of the experimentally measured unbinding force with the logarithm of the loading rate (Evans and Ritchie, 1997). Indeed, this theory has been proven through single-molecule experimental data (Evans and Ritchie, 1999; Merkel et al., 1999; Simson et al., 1999; Strunz et al., 1999; Pope et al., 2001; Brower-Toland et al., 2002). We expected that for the experiment described here the conditions under which the fibers were stretched would influence the forces required to disrupt DNA-protein interactions central to chromatin structure.

In a chromatin context it is evident that DNA-protein interactions must in some way be altered or disrupted for processes such as transcription and replication to occur. The effect of force on interactions that are central to chromatin structure is particularly relevant to force-generating motors that may be used to alter chromatin structure to gain access to the genetic code; for example RNA and DNA polymerases. In the study described here we collect data that allow us to determine both rupture force and length increase per event during the mechanical disruption of the chromatin fiber. We expect the force measurements to allow a study of the energetic barriers associated with chromatin disruption and the length measurements to aid in the identification of which interactions are disrupted for each individual event. Furthermore this technique may provide insight into pathways via which code access occurs. A detailed discussion of the potential of dynamic and static force spectroscopy studies of chromatin has been previously reported (Pope et al., 2002).

EXPERIMENTAL PROCEDURE

Materials

Biotinylated DNA was prepared using linearized bacteriophage λ-DNA (New England Biolabs, Beverly, MA), using the 12-base single-stranded overhangs at each end of the molecule. A 50-μg/ml solution of λ-DNA was incubated with 100 mM dGTP (Sigma, St. Louis, MO), 100 mM dCTP (Sigma), 0.3 mM bio-11-dUTP (Sigma), 0.4 mM bio-14-dATP (Gibco-BRL, Carlsbad, CA), and 10 U Klenow DNA polymerase (stock ~5 units/μl, Sigma) for 3 h at 37°C (50 mM phosphate buffer, 10 mM $MgCl_2$, pH 7.5). This promoted the synthesis of DNA strands filling in the 12-base-long overhang regions. After purification, λ-DNA, 16.4 μm in length, with two biotinylated bases at each 5′ end was obtained. A dilution of the DNA solution to 0.25 μg/ml in TE buffer (10 mM Tris-HCl, pH 7.5, 1 mM EDTA) was made for use in the experiments.

Streptavidin (SA)-coated (2.6 μm) polystyrene beads were prepared by incubating 2% of carboxylated beads (Bangs Laboratories, Fishers, IN) with 2 mg/ml of streptavidin (Roche Molecular Biochemical, Almere, The Netherlands) for 15 min at room temperature. 1-Ethyl-3-(3-dimethylaminopropyl)-carbodiimide (EDAC) (Sigma) was used to activate the carboxyl groups allowing covalent coupling between the bead and protein. The pH was adjusted to 6.5 and incubation was carried out either for 2 h at 37°C or overnight at room temperature. Glycine (100 mM) was used to block unreacted sites. Finally the beads were washed a number of times with 50 mM phosphate buffered saline, pH 7.5. A dilution of the beads to a final concentration of $\sim 10^5$ beads/ml in TE buffer was made for use in the optical tweezers experiment.

The main operating flow buffer used in the experiments was 10 mM Tris-HCl, pH 7.5, 1 mM EDTA, 150 mM NaCl, 0.05% BSA, and 0.01% NaN_3. BSA was used to prevent nonspecific attachment of cell extract proteins to the beads. During the chromatin fiber assembly process the main buffer was replaced with diluted *Xenopus laevis* egg extract (Leno, 1998); 12 μl of high-speed supernatant diluted in 1 ml of 50 mM HEPES-KOH, pH 7.6, 50 mM KCl, 1 mM EDTA, and 2 mM β-mercaptoethanol. After the chromatin fiber was assembled the diluted extract was carefully replaced with the main flow buffer.

Instrumentation and technique

The experimental setup and methods used to perform this study have been described in detail previously (Bennink et al., 2001a,b; Leuba et al., 2004). In brief, the setup comprises of a single-beam gradient optical trap generated using 1 W of a continuous wave laser (1064 nm, 2 W, Crystalaser, Reno, NV). The optical trap is used to catch one SA-functionalized bead. A custom-built flow cell, incorporating a fixed micropipette is mounted onto a piezo-driven *x-y* translation stage (Newport, Irvine, CA). This micropipette is used to catch and manipulate with high precision a second bead. Deflections of the transmitted light from the trapped bead are monitored using a quadrant detector. The two beads are observed by projection of the sample plane onto a charge-coupled device (CCD) camera. A semiautomated flow system is used to control the exchange of different solutions along with the rate of flow of these solutions through the flow chamber. A schematic of this arrangement is illustrated in Fig. 1.

Initially one end-biotinylated λ-phage DNA molecule is captured between two SA-functionalized beads. One bead is held at the tip of the micropipette and the second is held in the optical trap. A DNA force-extension curve is recorded by moving the micropipette bead away from the trapped bead. With increasing DNA tension, the trapped bead is pulled away from its zero-force position within the trap, and its displacement is accurately monitored using the quadrant detector. It should be noted that the optical trap stiffness (~100 pN/μm) is chosen such that in the force range under investigation the light falls on the detector within an area that has been predetermined to have a linear response. Force data are recorded for a DNA stretch-relax cycle along with an accurate length determination by monitoring the distance between the two beads during this cycle. The characteristic force extension behavior of a nontorsionally constrained dsDNA molecule is used to ensure that only one molecule is tethered between the two beads and the force plateau at 65 pN is used as a calibration for the trap stiffness (Cluzel et al., 1996; Smith et al., 1996).

Once a single molecule is suspended between the two beads, the optical trap is switched off and diluted egg extract is introduced into the flow chamber. A slow flow rate of ~50 μm/s is used to ensure that forces no greater than a few pN are exerted on the DNA molecule during the assembly. Videomicroscopy can be used to monitor the rate of compaction as a function

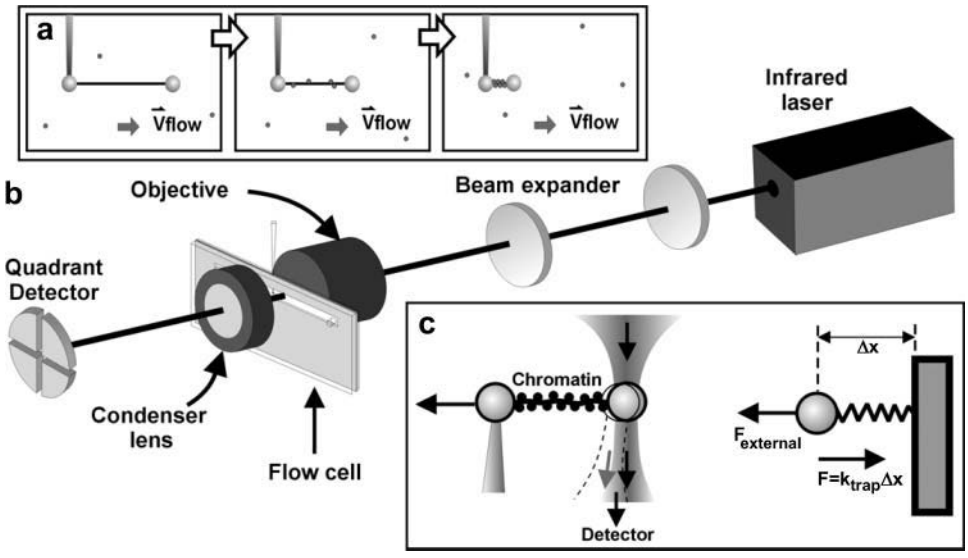

FIGURE 1 An illustration of the experimental setup. (*a*) After the capture of a single DNA molecule between two beads the *Xenopus* extract is added to the flow chamber. A very slow flow rate of <50 μm/s is used that corresponds to the application of low forces <1 pN on the DNA molecule. The molecule condenses from 16.4 to 2 μm in length. (*b*) The experimental setup comprises of a 1064-nm infrared laser, which is expanded to fill the back aperture of a water immersion objective lens. The objective focuses the laser to a spot in the center of the flow channel, hence establishing the optical trap. A piezo-driven flow cell with an integrated glass micropipette is employed to allow movement of the nontrapped bead. A CCD camera is used to track the distance between the two beads (not shown). A quadrant detector monitors deflections of the transmitted laser light from the trapped bead. (*c*) As the chromatin fiber is stretched the trapped bead is displaced by Δx from its zero-force position. This deflection is directly proportional to the tension within the molecule under investigation; hence the trap behaves as a simple Hookean spring for small bead displacements (<0.5 μm). It should be noted that the trap stiffness k_{trap} is chosen to ensure measurements are within the linear range of the detector ($k_{trap} \approx 100$ pN/μm).

of DNA tension. We have previously shown that assembly of the chromatin fiber is tension dependent and can be inhibited at forces >~10 pN (Bennink et al., 2001b). Under the lowest tension investigated, of ~1 pN, assembly was at a rate that corresponded to the formation of ~2–3 nucleosomes per second. The assembly process compacts the DNA molecule from 16.4 μm to an end point of ~2 μm. This is consistently observed in all experiments and hence reflects the compaction capabilities of this extract. Additional control experiments were carried out to ensure that the chromatin fiber did not attach itself nonspecifically to the beads.

Once the chromatin fiber is assembled and the normal flow buffer has replaced the cell extract, the laser is switched on and the freely suspended bead is carefully caught in the trap, ensuring minimum disturbance to the fiber structure. The fiber is stretched and relaxed at a constant velocity and force-versus-extension data are collected at a 2-kHz acquisition rate. Data are collected for a number of stretch-relax cycles of the same chromatin fiber. This is repeated a number of times for many different reconstituted fibers over apparent loading rates (product of optical trap stiffness and piezo velocity) ranging from 3.5 to 560 pN/s.

RESULTS AND ANALYSIS

Naked DNA has been well characterized in terms of its mechanical properties. In the low-force regime the molecule behaves as a worm-like chain (Bustamante et al., 1994; Marko and Siggia, 1995). At higher forces linear force-extension behavior is indicative of a simple Hookean spring behavior. At ~65 pN the molecule undergoes a highly cooperative transition to a stretched state that is ~1.7 times its original contour length (Smith et al., 1996; Cluzel et al., 1996). Fig. 2 *a* shows a typical force-extension curve for a single reconstituted chromatin fiber (*inset* is the second stretch-relax cycle for the same fiber). If we qualitatively compare the force-extension characteristics of the chromatin fiber to those of naked DNA we find that the stretch curve is very different. The 65-pN plateau, however, is still evident and the relaxation data are similar. The reconstituted chromatin fiber undergoes an initial stretch from which the mechanical properties of the intact fiber can be assessed. After this initial stretch a series of disruption events are observed. Tension within the fiber increases until a DNA-protein unbinding event occurs; at this instant a sharp drop in force is observed. Many of these events occur during the stretching of the fiber.

These discrete events can clearly be seen in the enlargement made from a small portion of the chromatin extension curve (Fig. 2 *b*). From each of these events a wealth of information can be extracted. For example, the force-extension data describe the mechanical properties of the fiber, and the rupture force, F, required to disrupt the interaction, provides information about the energetic penalties that must be overcome. As discussed earlier, a dynamic force spectroscopy study could be used to map both location and height of energy barriers in the unperturbed landscape, which would hence provide insight into the interaction kinetics. The change in contour length, ΔL_0, of the fiber due to the disruption event is an indication of the amount of DNA that is released, which in turn may be used to identify which interactions are broken.

Force-extension data were collected from a number of different reconstituted chromatin fibers that were stretched using different piezo pulling velocities. Considering that apparent loading rate is the product of the trap stiffness and piezo velocity, a visual examination of the chromatin stretch data was carried out. It was observed that although some data appeared to be consistent with higher rupture forces for increased loading rate conditions, this was not the case for all data sets. Instead the data showed a high degree of variability, which may reflect structural variations in the reconstituted fibers. Using custom-written LabView software the rupture force, F, and length change, ΔL_0, were measured for every DNA-protein unbinding event and for all of the chromatin force-extension curves.

An analysis of fiber length increase per DNA-protein unbinding event was carried out. Histograms of ΔL_0, plotted for each curve, revealed peaks that indicated discrete DNA length releases occurred during the force-induced disruption of the chromatin fibers. The positions of these peaks were determined using a multi-Gaussian fit to each histogram. These peak locations were then pooled together (locations

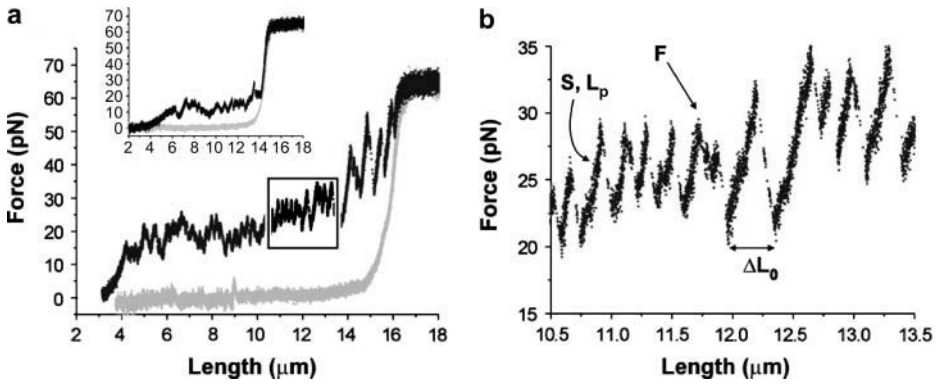

FIGURE 2 (*a*) The first and second (*inset*) stretch of a reconstituted chromatin fiber. The force-extension data were collected from a single DNA molecule incubated with *Xenopus* egg extract. The stretch curve is shown in black and the relax curve is shown in gray. (*b*) An enlargement of a small portion (*box* in panel *a*) of the chromatin stretch curve reveals discrete unbinding events, observed here as steps in the data. From each individual step information can be extracted about the mechanical properties of the fiber, such as persistence length (L_p) and stretch modulus (S). A study of rupture force (F) versus loading rate can be used to study the energetics and kinetics of interactions that are disrupted during the chromatin fiber stretch. The change in length for a single force value is essentially the change in fiber contour length ΔL_0, assuming that the mechanical properties of the fiber remain virtually unchanged after a single unbinding event.

from ~30 individual data sets of both first and later fiber stretches) and a histogram plot of these values was made (Fig. 3). A multi-Gaussian fit to this data revealed three peaks centered at values of 30, 59, and 117 nm. Note that values of 59 and 117 nm are consistent with earlier results for the unraveling of one or two nucleosomes, respectively (Bennink et al., 2001a). On the other hand, the 30-nm peak is consistent with the ''half-nucleosome'' unwrapping events observed by Brower-Toland (Brower-Toland et al., 2002). It is important to note that this study is the first to clearly observe all of these types of events during the opening of a single chromatin fiber.

Next we applied dynamic force spectroscopy theory to the rupture force data. Each chromatin fiber under investigation was considered as a linear array of individual nucleosomes, hence the model for multiple bonds loaded in series was used. We assume that each nucleosome has an equal probability of rupture and that rupture events within the array occur noncooperatively; the most probable rupture force, F^*, for nucleosome disruption may then be described as follows:

$$F^* = \frac{k_B T}{d}\left[\ln\left(\frac{1}{N}\frac{dF}{dt}\right) - \ln\left(\frac{k_B T k_{off}}{d}\right)\right], \qquad (1)$$

where d is the distance between the bound state and the activation barrier peak along the direction of the applied force, N is the number of nucleosomes in the array, dF/dt is the true loading rate, k_B is the Boltzman constant, T is absolute temperature, and k_{off} is the rate constant for bond disruption under zero external force (Evans, 1999, 2001). For each individual rupture event the true loading rate was calculated as the product of the slope of the data at the point of rupture (this takes into account the combined stiffness of the trap and the chromatin fiber itself) and the piezo velocity. The number of nucleosomes, N, comprising the array was determined from the contour length of the chromatin fiber (an estimate of the initial number of nucleosomes in the fiber was made, then for every 60-nm contour length increase it was assumed that one nucleosome was disrupted). When considering the disruption of a single molecular pair the $1/N$ term given in Eq. 1 is absent. It is included here because our chromatin fiber must be considered as a chain of N interacting pairs (DNA plus histones) in series (Evans, 2001; Brower-Toland et al., 2002). When N is large the probability that one of these molecular interactions will break is significantly greater than if N is small, hence this must be accounted for. Fig. 4 *a* shows a scatter plot of individual rupture force measurements versus the logarithm of the normalized true loading rate. This scatter plot was generated using all data from both first and later stretch curves. From this data two discrete force distributions were evident (these will be termed as high- and low-force distributions). Slices of data taken along the $\ln(1/N \quad dF/dt)$ axis (200 data points per slice; see *box*) were used to generate force histograms in which these two force distributions are clearly evident (Fig. 4 *a*, *inset*).

The rupture forces were next sorted and plotted depending on whether the stretch was the first stretch (Fig. 4 *b*) of the reconstituted fiber or subsequent (later) stretches (Fig. 4 *c*).

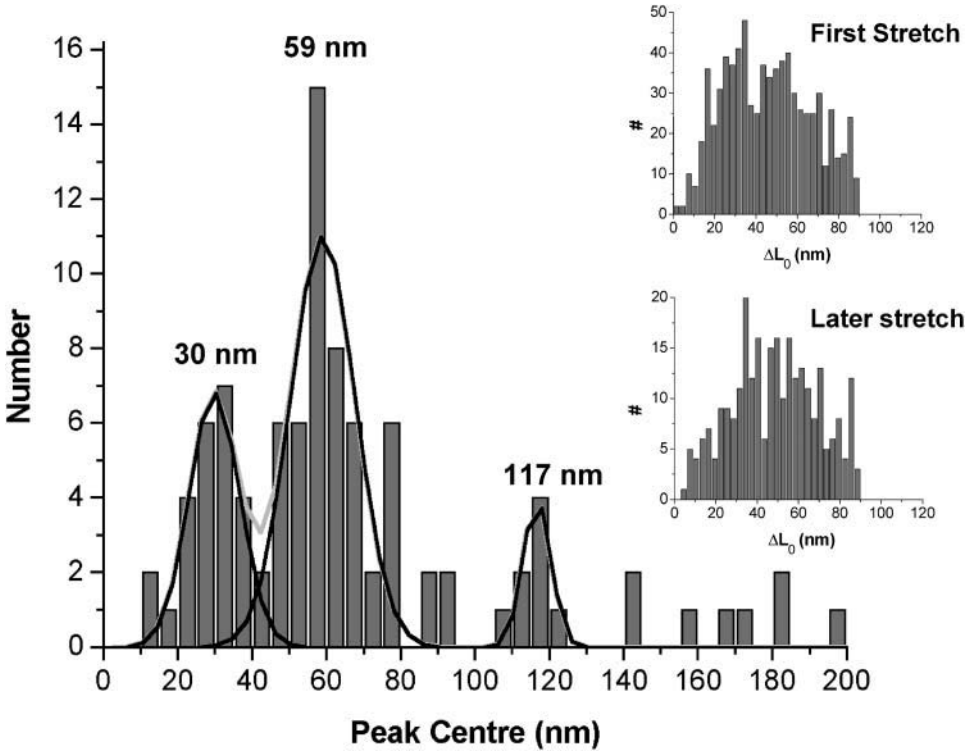

FIGURE 3 For each force-extension curve histogram plots of ΔL_0 revealed peaks corresponding to discrete length increments. Multi-Gaussian fits to these histograms were used to determine the center of these peaks. These values were then pooled together to produce the histogram shown here. A multi-Gaussian fit to this histogram revealed peaks located at 30 (mean ± SD 9, $n = 26$), 59 (mean ± SD 10, $n = 51$), and 117 (mean ± SD 5, $n = 8$) nm (accuracy of fit: $\chi^2 = 2.1$, $R^2 = 0.8$, $n = 97$). ΔL_0 values were also pooled together for both first and later fiber stretches (*inset*). It is clear from this data that there is little change in these distributions 30- and 60-nm events were observed in both cases with similar frequency.

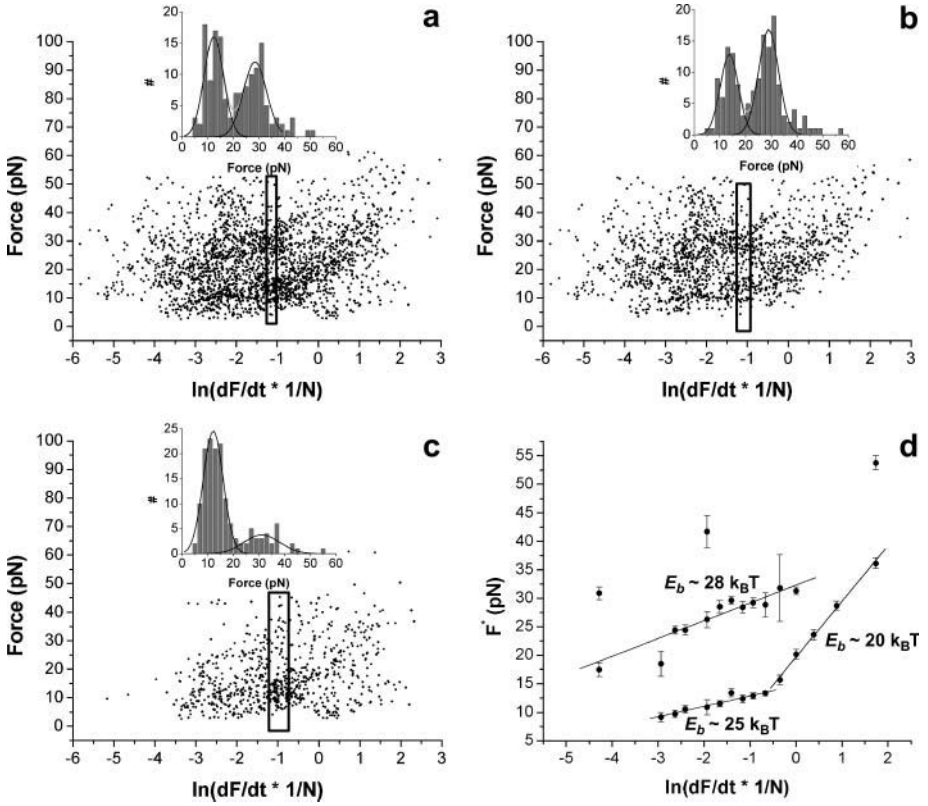

FIGURE 4 A plot of rupture forces versus $\ln(dF/dt \times 1/N)$ for (*a*) combined first and later stretches, (*b*) first stretches, and (*c*) later stretches of ~20 different chromatin fibers. Inset shows histogram plots of slices (see *boxes*) taken along the $\ln(dF/dt \times 1/N)$ axis through these data (200 data points per slice). Gaussian fits to these histograms reveal the most probable rupture forces F^*. (*d*) This plot was generated using the data shown in panel *a*. The plot of F^* versus the logarithm of the normalized loading rate reveals three linear regimes each corresponding to a different energy barrier as illustrated. Error bars represent the error in the histogram peak positions.

Similar to the combined data, the first stretch data also exhibited two discrete force distributions (*inset* histogram, generated from box data). Interestingly, however, for the later stretch data, the relative number of the high-force events was greatly reduced. This is clear from the histogram (Fig. 4 *c*, *inset*) where the high-force peak is significantly reduced relative to the low-force peak.

Using all of the data shown in Fig. 4 *a*, 200 data point slices were used to generate a series of histograms spanning the entire range in $\ln(1/N \quad dF/dt)$. The locations of the histogram force peaks were determined using multi-Gaussian fits. These peak positions indicated the most probable rupture force F^* for a given slice in $\ln(1/N \quad dF/dt)$. Fig. 4 *d* shows a plot of F^* versus the average value of $\ln(1/N \quad dF/dt)$. It is clear from the plot shown in Fig. 4 *d* that three linear F^* versus loading rate regimes exist. These three regimes represent three discrete energy barriers. Values of d and k_{off} corresponding to each of these barriers were obtained from linear fits to the data (see Eq. 1). The size of these energy barriers could next be determined using the following expression:

$$k_{off} = k_0 e^{-E_b/k_B T}. \quad (2)$$

Firstly it was necessary to estimate the unbinding attempt frequency ($k_0 = 1/\tau$). Considering the Kramers theory, the amount of time that it would take for two interacting objects to unbind is governed by viscous friction, γ_f, and the product of two length scales, $l_a\, l_{ts}$, where l_a is the confinement length in the bound state and l_{ts} is the impedance width of the transition state (Kramers, 1940).

$$\tau = l_a l_{ts}(\gamma_f/k_B T). \quad (3)$$

Here we consider that the crossing of energy barriers describing nucleosome unbinding events will involve the initial unwrapping of at least a few nanometers of DNA from the nucleosome (which is ~10 nm diameter). We hence estimate γ_f from Stokes drag on a sphere of dimensions ranging from 5 to 10 nm. Furthermore we estimate that both l_a and l_{ts} lie in the 1–5-nm range. Using these values in Eq. 3 an estimate of the prefactor k_0 (unbinding attempt frequency $1/\tau$) is made as $\sim 10^7\ s^{-1}$. Using Eqs. 1 and 2, the single energy barrier corresponding to the high-force distribution can be described by $d = 1.3 \pm 0.1$ nm, $k_{off} = (8.9 \pm 5.5)e^{-6}\ s^{-1}$, $E_b \approx 28\ k_B T$. The low-force distribution provides data for two individual energy barriers. For lower loading rates the energy barrier is measured as $d = 2.2 \pm 0.2$ nm, $k_{off} = (1.7 \pm 1.0)e^{-4}\ s^{-1}$, $E_b \approx 25\ k_B T$; for higher loading rates the second energy barrier is measured as $d = 0.41 \pm 0.02$ nm, $k_{off} = (1.4 \pm 0.1)e^{-2}\ s^{-1}$, $E_b \approx 20\ k_B T$. Considering that that value of k_0 lies in the range from 10^6 to $10^8\ s^{-1}$ the possible error in the values given for these energy barriers is $\sim 3\ k_B T$. To determine whether there was a correlation between these energy barriers and the type of interaction disrupted, the force data were sorted in relation to its corresponding energy barrier and correlation plots between F and ΔL_0 were generated. These plots showed very little correlation; both

the low-force and high-force data, corresponding to the 25 k_BT and 28 k_BT energy barriers, were consistent with a wide range of ΔL_0 (Fig. 5).

DISCUSSION

Our experiments reveal that chromatin assembled using *Xenopus laevis* egg extract, containing a range of enzymes similar to those found in vivo, shows a rich force spectroscopy of nucleosome disruption. We can make an initial assessment of our results based on the known composition of the chromatin fiber, along with our detailed knowledge of nucleosomal structure. It is known that the *Xenopus* extract used in this study contains a huge store of core histones, is deficient in linker histone H1, however does contain B4, an embryonic linker histone variant, and also contains HMG1 and HMG2 proteins (Wolffe, 1995). The high-speed supernatant assembles chromatin in vitro under physiological conditions and is known to result in physiologically spaced nucleosomal arrays, with one nucleosome per 180–190 bp (~62 nm) (Laskey et al., 1977; Glikin et al., 1984). This is identical to the spacing found in *Xenopus* chromatin. Assembly is mediated by histone chaperones. These chaperones shield the high positive charge of the histones from the DNA and allow regulated assembly of the fiber. Nucleoplasmin is one of the most abundant proteins in the extract and is known to act as a chaperone for the histone dimer H2A-H2B (Dilworth et al., 1987; Arnan et al., 2003). Similarly H3-H4 is bound to the peptide N1 until transfer and binding to the DNA molecule is achieved (Kleinschmidt and Franke, 1982; Dilworth et al., 1987). Once nucleosomes are formed along the DNA molecule they are then correctly spaced by chromatin remodeling factors (for a review on chromatin assembly, see Tyler, 2002).

Except for the core histones, other proteins within the extract are known to bind weakly to chromatin, hence it is likely that they will be washed away during the replacement of the cell extract by buffer (Felsenfeld and Groudine, 2003). We therefore expect only the strongly bound core histones and possibly linker histone B4 and HMG proteins to remain an integral part of the chromatin fibers under investigation. We may note that biochemical studies have shown that B4 is abundant in *Xenopus* early embryonic chromatin; hence we expect that the majority of nucleosomes contain linker histone B4 (Dimitrov et al., 1994). We should note that linker histone B4 is significantly different when compared to H1, in that the carboxyl terminal tail of B4 is much less basic, hence it is possible that B4 does not neutralize the negative charge of the linker DNA backbone as effectively, leading to a more extended chromatin fiber (Smith et al., 1988; Wolffe, 1995). HMG1 and HMG2 are small proteins having binding domains capable of spanning ~20 bp of DNA, which can bend the DNA through 130°. Although present within chromatin, their function remains unclear. It has been proposed that they may play a similar role to linker histone (Jackson et al., 1979), alternatively they may simply bind over short regions of naked DNA to neutralize the negatively charged DNA backbone and aid in the compaction process. It should also be noted that the assembled chromatin is enriched in phosphorylated and acetylated core histones and that these along with the linker histone variant B4, result in a chromatin structure that is in an open ''active'' structural conformation (Wolffe, 1995). Hence strong internucleosomal interactions are not expected.

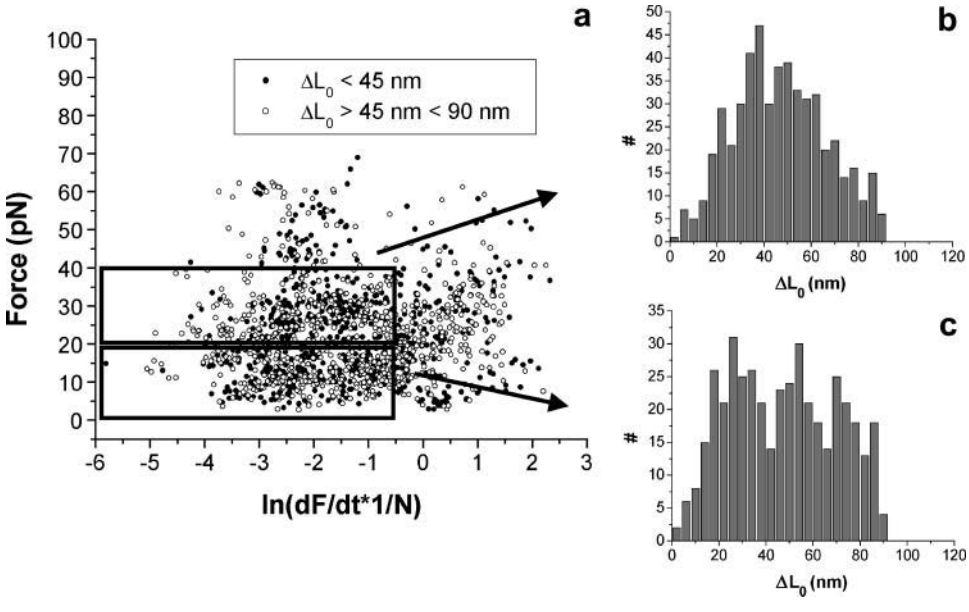

FIGURE 5 (*a*) Shows the same plot as that given in Fig. 4 *a*, however the data have been sorted to show force events corresponding to ΔL_0 values in the ranges of 0–45 nm (●) and 45–90 nm (○). It is considered that these data most likely correspond to 30- and 60-nm events, respectively. Both the open circles and solid circles are observed for both the high- and low-force distributions demonstrating a lack of correlation between event observed and energy barrier crossed. These data were further analyzed to generate the histograms in panels *b* and *c*. Values of $\ln(dF/dt*1/N) > -0.5$, corresponding to the 20 k_BT energy barrier, were not included in the analysis. The data were sorted as illustrated by the boxes and histograms of ΔL_0 were generated. (*b*) Shows ΔL_0 values corresponding to the ~28 k_BT energy barrier; (*c*) shows ΔL_0 values corresponding to the ~25 k_BT energy barrier (see Fig. 4 *d*).

The force-versus-extension data that we collect provide information about DNA-protein interactions that when disrupted involve a structural change that results in the release of DNA. Small proteins that are bound to the DNA, which do not wrap and compact the DNA, but simply bend it or act to shield electrostatic charge, may simply pop off (Baumann et al., 2000) or even smoothly deform (van Noort et al., 2004; Skoko et al., 2004) when tension is applied to the fiber and be removed without any detectable signal in the force-extension data. The HMG proteins are possible candidates for this type of behavior. From our discussion above on the composition of the chromatin fiber under investigation it seems reasonable to assume that the rupture events that we observe are likely to be almost exclusively due to nucleosome disruption, indeed this would result in significant and detectable changes in the length of the chromatin fiber.

Energetic penalties to chromatin disruption: two discrete force distributions

After the evaluation that the majority of events we observe are due to nucleosome disruption, we may consider why we observe two force distributions and why one of these distributions essentially disappears after the first fiber stretch. This observation may be explained by the presence or absence of linker histone in a nucleosome disruption event. If linker histone is present it is conceivable that nucleosome disruption will involve higher energetic penalties and rupture forces than for nonlinker-histone-containing nucleosomes. Since biochemical studies have demonstrated that nucleosomes may be disrupted in a stepwise manner simply through increasing salt concentration we are aware that the interactions involved in maintaining nucleosomal integrity are largely electrostatic. With increasing salt, the order in which the histones dissociate are firstly the linker histones, followed by the H2A-H2B dimers, and finally at high salt the $(H3\text{-}H4)_2$ tetramers are removed. Considering these observations we may expect that force-induced disruption of nucleosomes could also occur in a similar stepwise manner. Hence, the most weakly bound linker histones (in this case histone B4) could be removed first, either alone in which case the histone octamer would remain as an intact structural unit, or along with histone units such as H2A-H2B dimers, in which case a subnucleosomal particle would remain. Furthermore, in support of this idea, experiments that have tracked the mobility of linker histone H1 inside the cell nucleus have shown that they are weakly bound and are highly mobile proteins (Misteli et al., 2000; Lever et al., 2000). The data can hence be interpreted such that the two force regimes represent nucleosomes that do (high-force data) and do not (low-force data) contain linker histone and that the first stretch results in the removal of almost all linker histones, hence the high-force distribution essentially disappears. It may be noted that the data we present are consistent with a stoichiometry of approximately one B4 per two nucleosomes. If we examine the first stretch of the data shown in Fig. 4 *b* (*inset* histogram) it is clear that there are approximately equal numbers of events corresponding to the low- and high-force distributions. A stoichiometry of one B4 per two nucleosomes seems reasonable considering that biochemical characterization reveals that B4 is abundant in *Xenopus* early embryonic chromatin (Dimitrov et al., 1994).

We next applied dynamic force spectroscopy theory to the two discrete force distributions in Fig. 4. In the case of the high-force distribution we observe a single energy barrier $\sim 28\ k_BT$ in height. For the low-force distribution we observe two different energy barriers that are $\sim 25\ k_BT$ and $\sim 20\ k_BT$ in height, for low and high loading rates, respectively. The barriers that we expect to be most significant in terms of energetic penalties that need to be overcome in the unperturbed natural system are those that are measured at very low loading rate, hence the $\sim 28\ k_BT$ and the $\sim 25\ k_BT$ barriers. It is interesting that the events corresponding to the $\sim 28\ k_BT$ barrier are diminished after the first stretch of the fiber. Because we propose that after the first fiber stretch the majority of linker histones are removed, the $\sim 28\ k_BT$ and $\sim 25\ k_BT$ nucleosome disruption events may correspond to nucleosomes that do or do not contain linker histone, respectively. The difference of $\sim 3\ k_BT$ between these two barriers may therefore provide an estimate of the binding energy contribution of the embryonic linker histone B4 to the stability of the nucleosome.

Furthermore, it is interesting to compare our results to those of an earlier similar study (Brower-Toland et al., 2002) where a single energy barrier was measured for a nucleosome disruption event corresponding to the release of ~27 nm of DNA. This energy barrier was reported to have a height of $E_b = 36\text{–}38\ k_BT$, $d = 3.2$ nm, and $k_{off} = 3e^{-7}\ s^{-1}$. This energy barrier is clearly larger than those measured here in this study. However, this may not be too surprising considering the differences between the two studies. Firstly a nucleosome positioning DNA sequence is used, which is likely to have a $\Delta\Delta G$ of $\sim -1\ k_BT$ compared to that of random sequence DNA (Thåström et al., 2004). Also different salt conditions are used: 100 mM NaCl plus 1.5 mM $MgCl_2$ compared to 150 mM NaCl used here. Furthermore, the calculation of barrier height requires an estimation of the unbinding attempt frequency. Our estimation of k_0 at $10^7\ s^{-1}$ is two or more orders of magnitude different from the analysis of Brower-Toland et al. (2002), which would account for an additional difference in ΔG of $\sim -6\ k_BT$.

Unraveling DNA from the nucleosome

Measurement of change in contour length ΔL_0 per disruption event revealed that these events clearly involved the release of two discrete DNA lengths of 30 and 60 nm. This poses the question of which nucleosome interactions could be disrupted

to result in the release of these discrete lengths. Considering that nucleosomal structure may under applied force be disrupted in a stepwise manner, a single observed event could involve the dissociation of: 1), linker histone alone; 2), linker histone plus one H2A-H2B dimer; 3), linker histone plus both H2A-H2B dimers; 4), linker histone plus the core histone octamer; 5), one H2A-H2B dimer; 6), two H2A-H2B dimers; 7), $(H3\text{-}H4)_2$ tetramer; 8), hexamer of $(H3\text{-}H4)_2$ plus one H2A-H2B dimer; and 9), core histone octamer. If we consider the structure of the nucleosome in greater detail we know that the histone tetramer alone wraps 120 bp (~40 nm) of DNA, the octamer stably wraps 146 bp (~49 nm) of DNA and the association of linker histone can extend and stabilize histone-DNA interactions over 160 bp (~54 nm).

From the x-ray crystal structure of the nucleosome an assessment of the interactions between the DNA and histone proteins can be made (Fig. 6) (Luger et al., 1997; Luger and Richmond, 1998). DNA is known to wrap in a left-handed superhelix along grooves in the octamer structure. With each turn of the helix close contacts are made where the DNA minor groove faces inwards to the octamer surface (every ~10 bp). The histones are bound in a symmetrical manner, H2A-H2B dimers are located at the periphery where DNA enters and exits the nucleosome and $(H3\text{-}H4)_2$ is found at the central bound DNA region. The strongest interactions are found between the $(H3\text{-}H4)_2$ tetramer and the DNA at the most central region located at the dyad position. The reconstituted chromatin fiber is known to have nucleosomes spaced by ~185 bp (~62 nm). We can therefore postulate from this assessment that the 60-nm events are likely to correspond to the disruption of entire nucleosomes involving the release of core-histone-bound DNA and linker-histone-bound DNA. Furthermore, the 30-nm events would correspond to partial nucleosome disruption events. An assessment of length releases associated with a stepwise disruption of individual nucleosomes is illustrated in Fig. 6 and Table 1. It should be noted that the release of linker DNA is also included in this model. Although linker DNA is not considered tightly bound to the histone proteins, it is known that interactions may be established with the histone tails (Luger, 2003). This in combination with geometric constraints that nucleosome structure imposes on the direction of the path from one nucleosome to the next is expected to result in an extra contribution to the ΔL_0 value measured from the data. Although we present values corresponding to the release of the full length of linker DNA, we expect that these values will in fact be a few nanometers less. This is actually observed in our experimental data (compare the experimental 59 nm with the model value of 62 nm for the disruption of a full nucleosome).

From this assessment we can propose two different models for nucleosome disruption. The first ''new'' model suggests that nucleosomes may be disrupted whereby DNA bound to linker histone and one H2A-H2B dimer is released first, followed by the release of the remaining histone-hexamer-bound DNA. This model is further supported by AFM data of

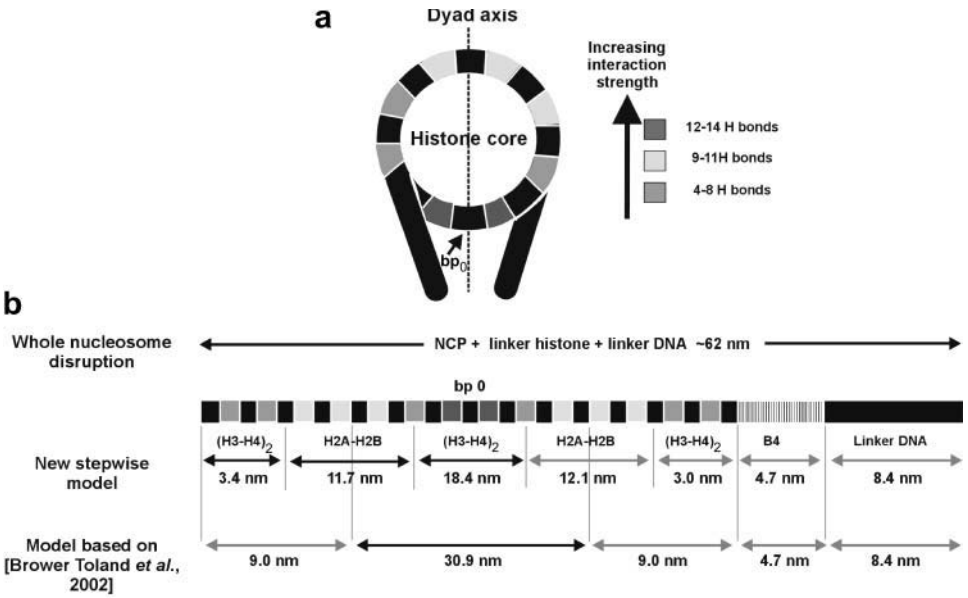

FIGURE 6 (*a*) Simplified representation of interactions between DNA and the core histone proteins, based on a high-resolution x-ray crystallography study of the NCP (Luger et al., 1997). The number of hydrogen bonds formed at each interaction location is shown (found for ~10 bp intervals at locations where the minor groove of the DNA double helix turns inwards toward the protein core) and gives an estimation of relative interaction strengths at these locations. (*b*) Illustrated is nucleosome bound DNA stretched out in one direction. From left to right we observe the interaction ''hot spots'' starting with interactions between the DNA and $(H3\text{-}H4)_2$ tetramer. The eight histone proteins interact in such a way that a groove is formed along the octamer surface to which the DNA is able to bind. The path of the DNA along this groove is such that the DNA-histone interactions sites alternate between $(H3\text{-}H4)_2$ and H2A-H2B. The experimentally observed DNA length increments are consistent with either the loss of a full nucleosome or with a stepwise nucleosome disruption. Two possible stepwise nucleosome disruption models that could be used to interpret the data are illustrated. The first ''new model'' shows that the experimentally observed DNA length increments are consistent with the stepwise loss of linker histone plus one H2A-H2B dimer (*gray arrows*) followed by the loss of the H2A-H2B.$(H3\text{-}H4)_2$ hexamer (*black arrows*). The second model is based on an earlier model, which proposes unpeeling of weakly bound DNA from the entry-exit locations of the NCP (*gray arrows*). Followed by disruption of the tightly bound DNA symmetrical about the dyad axis of the nucleosome (*black arrows*). Possible DNA length releases for our chromatin fiber based on these two models are given in Table 1.

TABLE 1 Shows possible DNA length releases expected based on the models illustrated in Fig. 6

New nucleosome disruption model	DNA length release (nm) stage 1		DNA length release (nm) stage 2
Unraveling of linker histone, linker DNA, and histone octamer	61.7		
Unraveling of linker histone, linker DNA, and H2A-H2B dimer	28.2	Followed by hexamer unraveling H2A-H2B.$(H3\text{-}H4)_2$	33.5
Model based on (Brower Toland et al., 2002)			
Unraveling of linker histone, linker DNA, and weakly bound NCP DNA	30.8	Loss of strongly bound NCP DNA	30.9

arrays of subnucleosomal particles that show the stable wrapping of ~25 nm as compared to ~50 nm per full nucleosomal particle (Nikova et al., 2004). The second model, based on an earlier proposed model (Brower-Toland et al., 2002), suggests that DNA bound to linker histone plus DNA that is weakly bound within the NCP is released first, followed by the release of the remaining strongly bound DNA from the core histone octamer. Furthermore, the core histone proteins may not necessarily be completely removed from the DNA molecule, hence the DNA may rebind to histones that remain bound upon relaxation of the fiber. Indeed, this effect is consistent with our own observations. Although the fiber is extended beyond the contour length of the naked DNA molecule, relaxation of the fiber results in a new fiber of intermediate length between that of the initial fiber and that of naked DNA. From our rupture signatures it is evident that this new fiber consists of intact nucleosomes and possibly subnucleosomal particles. This effect was also reported in the study of Brower-Toland (Brower-Toland et al., 2002). It was suggested that the strong DNA-histone interactions that span 11 bp at the dyad position (bp_0; Fig. 6) are sufficient to keep the histone octamer bound to the DNA (Brower-Toland et al., 2002). The same could also apply to a histone hexamer, H2A-H2B.$(H3\text{-}H4)_2$ or tetramer, $(H3\text{-}H4)_2$. A simple requirement for nucleosome refolding is that not all of the DNA-histone interactions are broken during the fiber stretch.

One question that may be asked is whether a half-disrupted nucleosome is less stable than an intact nucleosome. Hence if so it would be expected that after a nucleosome is ''half-disrupted'' continued pulling of the chromatin fiber would be more likely to pull the rest of the same nucleosome apart resulting in pairing of the 30-nm rupture steps. An analysis of the sequence in which the 30-nm and 60-nm steps occur was carried out for 14 different data sets, with the result that no sequence correlations were found.

To assess whether these two different rupture signatures of 30 and 60 nm could also be assigned characteristic energy barriers, a correlation analysis was carried out. These data, however, revealed little correlation because both the low- and high-force data distributions were found to be associated with both rupture lengths. This result provides further support to the idea that the high- and low-force distributions rather correspond to nucleosomes with and without linker histone bound, respectively.

CONCLUSIONS

Previous studies have observed ~60 and ~120 nm events (one and two nucleosome removals) during force-induced disruption of chromatin fibers assembled using *Xenopus* egg extracts (Bennink et al., 2001a) and ~30 nm (half-nucleosome) events during the disruption of fibers assembled using purified histones via salt dialysis (Brower-Toland et al., 2002). This is the first study where both of these types of events have been observed for a single chromatin fiber. Here we show that by studying a range of different loading rates, nucleosomes may unravel either in a single step as whole entities, or in a stepwise manner that may involve the loss of some of the core histones from the octamer. Despite significant differences in composition between the reconstituted chromatin fiber and the short nucleosomal array recently studied (Brower-Toland et al., 2002), our results show that both systems can show the ~30 nm half-nucleosome events. Furthermore, a loading rate analysis of disruption forces revealed three individual energy barriers, ~20 k_BT, ~25 k_BT, and ~28 k_BT in height. For subsequent stretches of the fiber it was found that events corresponding to the ~28 k_BT energy barrier were significantly reduced. We propose that this reduction in the ~28 k_BT events corresponds to the loss of weakly bound linker histone B4 during the first stretch of the fiber. We estimate that the energetic contribution of B4 to nucleosome stability is ~3 k_BT.

These results provide important knowledge about the energetic barriers that must be overcome to access DNA within a relatively open structure. The technique of force-induced disruption of chromatin that we employ here is of particular relevance to DNA template-dependent processes that involve force-exerting molecular motors. Single-molecule studies on bare DNA templates have revealed that enzymes such as DNA and RNA polymerases are capable of exerting forces that are on the order of tens of piconewtons. (Yin et al., 1995; Wang et al., 1998). Furthermore, experiments have previously shown that transcription is unhindered by $(H3\text{-}H4)_2$ histone tetramers bound to DNA (Tremethick et al., 1990; Wolffe, 1989). Hence it is very likely that access to the genetic code involves a cleverly orchestrated mechanism through which nucleosomal structure may be disrupted and efficiently reformed behind the transcription/replication machinery. This mechanism may occur in a single or multistage process involving the initial

loss of linker histone and/or H2A-H2B dimers. Furthermore, the exact nature of this process may be governed by the magnitude of the force exerted by the molecular motor. It is interesting to note that for either force or torque to be exerted on chromatin by a molecular motor would require motion constraints, for example, by anchoring polymerase to the nuclear matrix or to other nuclear bodies.

An obvious continuation from these studies would be to replace or remove different components in the cell extract system to assess their role in chromatin structure and stability. For example, the exchange of embryonic linker histone B4 for somatic linker histone H1, or simply the complete removal of B4, could be investigated. The role of histone modifications could be studied by replacement with specifically modified recombinant histones. The role of histone tails in stabilizing chromatin structure could be studied by a comparison with tail-less histones. Also of unknown significance is the role of nonhistone structural proteins such as the HMG proteins. It is clear that the folding of DNA into chromatin presents many structural impediments to any nuclear process that requires access to the genetic code. Despite this extensive compaction, complex processes such as transcription, replication, recombination, and repair occur efficiently in a chromatin environment. Single-molecule studies such as optical tweezers promise a further insight into chromatin structure and function.

The authors gratefully acknowledge G. Leno for the kind gift of *Xenopus Laevis* egg extract (prepared by Z. H. Lu).

Presented research is supported by the Dutch Foundation for Fundamental Research on Matter (L.H.P.) and by National Science Foundation grants DMR-0203963 and BIO-MCB-0240998 (L.H.P. and J.F.M.).

REFERENCES

Arnan, C., N. Saperas, C. Prieto, M. Chiva, and J. Ausió. 2003. Interaction of nucleoplasmin with core histones. *J. Biol. Chem.* 278:31319–31324.

Baumann, C. G., V. A. Bloomfield, S. B. Smith, C. Bustamante, M. D. Wang, and S. M. Block. 2000. Stretching of single collapsed DNA molecules. *Biophys. J.* 78:1965–1978.

Bednar, J., R. A. Horowitz, J. Dubochet, and C. L. Woodcock. 1995. Chromatin conformation and salt-induced compaction: three-dimensional structural information from cryoelectron microscopy. *J. Cell Biol.* 131: 1365–1376.

Bednar, J., R. A. Horowitz, S. A. Grigoryev, L. M. Carruthers, J. C. Hansen, A. J. Koster, and C. L. Woodcock. 1998. Nucleosomes, linker DNA, and linker histone form a unique structural motif that directs the higher order folding and compaction of chromatin. *Proc. Natl. Acad. Sci. USA.* 95:14173–14178.

Bennink, M. L., S. H. Leuba, G. H. Leno, J. Zlatanova, B. G. de Grooth, and J. Greve. 2001a. Unfolding individual nucleosomes by stretching single chromatin fibers with optical tweezers. *Nat. Struct. Biol.* 8:606–610.

Bennink, M. L., L. H. Pope, S. H. Leuba, B. G. de Grooth, and J. Greve. 2001b. Single chromatin fibre assembly using optical tweezers. *Single Mol.* 2:91–97.

Brower-Toland, B. D., C. L. Smith, R. C. Yeh, J. T. Lis, C. L. Peterson, and M. D. Wang. 2002. Mechanical disruption of individual nucleosomes reveals a reversible multistage release of DNA. *Proc. Natl. Acad. Sci. USA.* 99:1960–1965.

Bustamante, C., J. F. Marko, E. D. Siggia, and S. B. Smith. 1994. Entropic elasticity of λ-phage DNA. *Science.* 265:1599–1600.

Bustamante, C., G. Zuccheri, S. H. Leuba, G. Yang, and B. Samori. 1997. Visualization and analysis of chromatin by scanning force microscopy. *Methods.* 12:73–83.

Clark, D. J., and T. Kimura. 1990. Electrostatic mechanism of chromatin folding. *J. Mol. Biol.* 211:883–896.

Cluzel, P., A. Lebrun, C. Heller, R. Lavery, J.-L. Viovy, D. Chatenay, and F. Caron. 1996. DNA: an extensible molecule. *Science.* 271:792–794.

Cox, L. S., and R. A. Laskey. 1991. DNA replication occurs at discrete sites in pseudonuclei assembled from purified DNA in vitro. *Cell.* 66:271–275.

Cui, Y., and C. Bustamante. 2000. Pulling a single chromatin fiber reveals the forces that maintain its higher-order structure. *Proc. Natl. Acad. Sci. USA.* 97:127–132.

Dilworth, S. M., S. J. Black, and R. A. Laskey. 1987. Two complexes that contain histones are required for nucleosome assembly in vitro: role of nucleoplasmin and N1 in Xenopus egg extracts. *Cell.* 51:1009–1018.

Dimitrov, S., M. C. Dasso, and A. P. Wolffe. 1994. Remodelling sperm chromatin in Xenopus laevis egg extracts: the role of core histone phosphorylation and linker histone B4 in chromatin assembly. *J. Cell Biol.* 126:591–601.

Evans, E. 1999. Energy landscapes of biomolecular adhesion and receptor anchoring at interfaces explored with dynamic force spectroscopy. *Faraday Discuss.* 111:1–16.

Evans, E. 2001. Probing the relation between force—lifetime—and chemistry in single molecular bonds. *Annu. Rev. Biophys. Biomol. Struct.* 30:105–128.

Evans, E., and K. Ritchie. 1997. Dynamic strength of molecular adhesion bonds. *Biophys. J.* 72:1541–1555.

Evans, E., and K. Ritchie. 1999. Strength of a weak bond connecting flexible polymer chains. *Biophys. J.* 76:2439–2447.

Felsenfeld, G., and M. Groudine. 2003. Controlling the double helix. *Nature.* 421:448–453.

Finch, J. T., and A. Klug. 1976. Solenoidal model for superstructure in chromatin. *Proc. Natl. Acad. Sci. USA.* 73:1897–1901.

Forbes, D. J., M. W. Kirschner, and J. W. Newport. 1983. Spontaneous formation of nucleus-like structures around bacteriophage DNA microinjected into *Xenopus* eggs. *Cell.* 34:13–23.

Garcia-Ramirez, M., F. Dong, and J. Ausio. 1992. Role of the histone ''tails'' in the folding of oligonucleosomes depleted of histone H1. *J. Biol. Chem.* 267:19587–19595.

Glikin, G. C., I. Ruberti, and A. Worcel. 1984. Chromatin assembly in *Xenopus* oocytes: in vitro studies. *Cell.* 37:33–41.

Hansen, J. C., J. Ausió, V. H. Stanik, and K. E. van Holde. 1989. Homogeneous reconstituted oligonucleosomes, evidence for salt-dependent folding in the absence of histone H1. *Biochemistry.* 28:9129–9136.

Hansen, J. C., and A. P. Wolffe. 1992. The influence of chromatin folding on transcription initiation and elongation by RNA polymerase III. *Biochemistry.* 31:7977–7988.

Horowitz, R. A., D. A. Agard, J. W. Sedat, and C. L. Woodcock. 1994. The three-dimensional architecture of chromatin in situ: electron tomography reveals fibers composed of a continuously variable zig-zag nucleosomal ribbon. *J. Cell Biol.* 125:1–10.

Jackson, J. B., J. M. Pollock, Jr., and R. L. Rill. 1979. Chromatin fractionation procedure that yields nucleosomes containing near-stoichiometric amounts of high mobility group non histone chromosomal proteins. *Biochemistry.* 18:3739–3748.

Kleinschmidt, J. A., and W. W. Franke. 1982. Soluble acidic complexes containing histones H3 and H4 in nuclei of Xenopus laevis oocytes. *Cell.* 29:799–809.

Kramers, H. A. 1940. Brownian motion in a field of force and the diffusion model of chemical reactions. *Physica (Utrecht).* 7:284–304.

Ladoux, B., J.-P. Quivy, P. Doyle, O. du Roure, G. Almouzni, and J.-L. Viovy. 2000. Fast kinetics of chromatin assembly revealed by single-molecule videomicroscopy and scanning force microscopy. *Proc. Natl. Acad. Sci. USA.* 97:14251–14256.

Laitinen, J., K. Stenius, T. O. Eloranta, and E. Holtta. 1998. Polyamines may regulate S-phase progression but not the dynamic changes of chromatin during the cell cycle. *J. Cell. Biochem.* 68:200–212.

Laskey, R. A., A. D. Mills, and N. R. Morris. 1977. Assembly of SV40 chromatin in a cell-free system from Xenopus eggs. *Cell.* 10:237–243.

Leno, G. H. 1998. Cell-free systems to study chromatin remodeling. *Methods Cell Biol.* 53:497–515.

Leuba, S. H., M. L. Bennink, and J. Zlatanova. 2004. Single-molecule analysis of chromatin. *Methods Enzymol.* 376:73–105.

Leuba, S. H., C. Bustamante, K. van Holde, and J. Zlatanova. 1998b. Contributions of linker histones and histone H3 to chromatin structure: scanning force microscopy studies on trypsinized fibers. *Biophys. J.* 74: 2823–2829.

Leuba, S. H., C. Bustamante, J. Zlatanova, and K. van Holde. 1998a. Linker histone tails and N-tails of histone H3 are redundant: scanning force microscopy studies of reconstituted fibers. *Biophys. J.* 74:2830–2839.

Leuba, S. H., G. Yang, C. Robert, B. Samori, K. van Holde, J. Zlatanova, and C. Bustamante. 1994. Three-dimensional structure of extended chromatin fibers as revealed by tapping-mode scanning force microscopy. *Proc. Natl. Acad. Sci. USA.* 91:11621–11625.

Lever, M. A., J. P. H. Th'ng, X. Sun, and M. J. Hendzel. 2000. Rapid exchange of histone H1.1 on chromatin in living cells. *Nature.* 408:873–876.

Luger, K. 2003. Structure and dynamic behaviour of nucleosomes. *Curr. Opin. Genet. Dev.* 13:127–135.

Luger, K., A. W. Meader, R. K. Richmond, D. F. Sargent, and T. J. Richmond. 1997. X-ray structure of the nucleosome core particle at 2.8 Å resolution. *Nature.* 389:251–259.

Luger, K., and T. J. Richmond. 1998. DNA binding within the nucleosome core. *Curr. Opin. Struct. Biol.* 8:33–40.

Marko, J. F., and E. D. Siggia. 1995. Stretching DNA. *Macromolecules.* 28:8759–8770.

Merkel, R., P. Nassoy, A. Leung, K. Ritchie, and E. Evans. 1999. Energy landscapes of receptor-ligand bonds explored with dynamic force spectroscopy. *Nature.* 397:50–53.

Misteli, T., A. Gunjan, R. Hock, M. Bustin, and D. T. Brown. 2000. Dynamic binding of histone H1 to chromatin in living cells. *Nature.* 408:877–881.

Nikova, D., L. H. Pope, M. L. Bennink, K. A. van Leijenhorst-Groener, K. van der Werf, and J. Greve. 2004. Unexpected binding motifs for subnucleosomal particles revealed by atomic force microscopy. *Biophys. J.* 6:4135–4145.

Pope, L. H., M. L. Bennink, and J. Greve. 2002. Optical tweezers stretching of chromatin. *J. Muscle Res. Cell Motil.* 23:397–407.

Pope, L. H., M. C. Davies, C. A. Laughton, C. J. Roberts, S. J. B. Tendler, and P. M. Williams. 2001. Force-induced melting of a short DNA double helix. *Eur. Biophys. J.* 30:53–62.

Schwarz, P. M., and J. C. Hansen. 1994. Formation and stability of higher order chromatin structures. *J. Biochem. (Tokyo).* 269:16284–16298.

Simson, D. A., M. Strigl, M. Hohenadl, and R. Merkel. 1999. Statistical breakage of single protein A-IgG bonds reveals crossover from spontaneous to force-induced bond dissociation. *Phys. Rev. Lett.* 83: 652–655.

Skoko, D., B. Wong, R. Johnson, and J. F. Marko. 2004. Micromechanical analysis of the binding of DNA-bending proteins HMGB1, NHP6A and HU reveals their ability to cooperatively form highly stable DNA-protein complexes. *Biochemistry.* 43:13867–13874.

Smith, S. B., Y. Cui, and C. Bustamante. 1996. Overstretching B-DNA: the elastic response of individual double-stranded and single-stranded DNA molecules. *Science.* 271:795–799.

Smith, R. C., E. Dworkin-Rastl, and M. D. Dworkin. 1988. Expression of a histone H1-like protein is restricted to early Xenopus development. *Genes Dev.* 2:1284–1295.

Strunz, T., K. Oroszlan, R. Schäfer, and H. Guntherödt. 1999. Dynamic force spectroscopy of single DNA molecules. *Proc. Natl. Acad. Sci. USA.* 96:11277–11282.

Thåström, A., P. T. Lowary, and J. Widom. 2004. Measurement of histone-DNA interaction free energy in nucleosomes. *Methods.* 33:33–44.

Tremethick, D., K. Zucker, and A. Worcel. 1990. The transcription complex of the 5 S RNA gene, but not transcription factor IIIA alone, prevents nucleosomal repression of transcription. *J. Biol. Chem.* 265: 5014–5023.

Tyler, J. 2002. Chromatin assembly: cooperation between histone chaperones and ATP-dependent nucleosome remodelling machines. *Eur. J. Biochem.* 269:2268–2274.

van Holde, K. E. 1989. Chromatin. Springer-Verlag, New York. 111–148.

van Noort, J., S. Verbrugge, N. Goosen, C. Dekker, and R. T. Dame. 2004. Dual architectural roles of HU: formation of flexible hinges and rigid filaments. *Proc. Natl. Acad. Sci. USA.* 101:6969–6974.

Wang, M., M. J. Schnitzer, H. Yin, R. Landick, J. Gelles, and S. M. Block. 1998. Force and velocity measured for single molecules of RNA polymerase. *Science.* 282:902–907.

Widom, J., and A. Klug. 1985. Structure of the 300 Å chromatin filament: x-ray diffraction from oriented samples. *Cell.* 43:207–213.

Wolffe, A. 1995. Chromatin structure and function. Academic Press Limited, London, UK.

Wolffe, A. P. 1989. Dominant and specific repression of Xenopus oocyte 5S RNA genes and satellite I DNA by histone H1. *EMBO J.* 8:527–537.

Yin, H., M. D. Wang, K. Svoboda, R. Landick, S. M. Block, and J. Gelles. 1995. Transcription against an applied force. *Science.* 270:1653–1657.

Yodh, J. G., N. Woodbury, L. S. Shlyakhtenko, Y. L. Lyubchenko, and D. Lohr. 2002. Mapping nucleosome locations on the 208-12 by AFM provides clear evidence for cooperativity in array occupation. *Biochemistry.* 42:3565–3574.